8-15-2021

Differential classification of states of consciousness using envelope- and phase-based functional connectivity

Catherine Duclos

Michael S Avidan

et al.

Differential classification of states of consciousness using envelope- and phase-based functional connectivity

Catherine Duclos [a,b], Charlotte Maschke [a,c], Yacine Mahdid [a,c], Kathleen Berkun [d], Jason da Silva Castanheira [b,c], Vijay Tarnal [e], Paul Picton [e], Giancarlo Vanini [e], Goodarz Golmirzaie [e], Ellen Janke [e], Michael S. Avidan [f], Max B. Kelz [g], Lucrezia Liuzzi [h], Matthew J. Brookes [i], George A. Mashour [e], Stefanie Blain-Moraes [a,b,*]

[a] Montreal General Hospital, McGill University Health Centre, 1650 Cedar Ave, Montreal, QC, Canada
[b] School of Physical and Occupational Therapy, McGill University, 3654 Promenade Sir-William-Osler Montreal, Quebec H3G 1Y5, Canada
[c] Integrated Program in Neuroscience, McGill University, 3801 University Street, Montreal Quebec H3A 2B4, Canada
[d] Section on Behavioral Neuroscience, National Institutes of Health, 9000 Rockville Pike, Bethesda, MD 20892 United States
[e] Center for Consciousness Science and Department of Anesthesiology, 1301 Catherine Street, 4102 Medical Science 1, University of Michigan Medical School, Ann Arbor, MI 48109 United States
[f] Department of Anesthesiology, Washington University School of Medicine, 660 S. Euclid Ave. St. Louis, MO 63110 United States
[g] Department of Anesthesiology, Perelman School of Medicine, University of Pennsylvania, 3400 Spruce St, Philadelphia, PA 19104 United States
[h] Mood Brain and Development Unit, Emotion and Development Branch, National Institute of Mental Health, National Institutes of Health, 9000 Rockville Pike, Bethesda, MD 20892 United States
[i] Sir Peter Mansfield Imaging Centre, School of Physics and Astronomy, University of Nottingham, Nottingham, NG7 2RD United Kingdom

ARTICLE INFO

ABSTRACT

The development of sophisticated computational tools to quantify changes in the brain's oscillatory dynamics across states of consciousness have included both envelope- and phase-based measures of functional connectivity (FC), but there are very few direct comparisons of these techniques using the same dataset. The goal of this study was to compare an envelope-based (i.e. Amplitude Envelope Correlation, AEC) and a phase-based (i.e. weighted Phase Lag Index, wPLI) measure of FC in their classification of states of consciousness. Nine healthy participants underwent a three-hour experimental anesthetic protocol with propofol induction and isoflurane maintenance, in which five minutes of 128-channel electroencephalography were recorded before, during, and after anesthetic-induced unconsciousness, at the following time points: *Baseline;* light sedation with propofol (*Light Sedation*); deep unconsciousness following three hours of surgical levels of anesthesia with isoflurane *(Unconscious);* five minutes prior to the recovery of consciousness *(Pre-ROC);* and three hours following the recovery of consciousness (*Recovery)*. Support vector machine classification was applied to the source-localized EEG in the alpha (8–13 Hz) frequency band in order to investigate the ability of AEC and wPLI (separately and together) to discriminate i) the four states from *Baseline*; ii) *Unconscious* ("deep" unconsciousness) vs. *Pre-ROC* ("light" unconsciousness); and iii) responsiveness (*Baseline, Light Sedation, Recovery)* vs. unresponsiveness (*Unconscious, Pre-ROC)*. AEC and wPLI yielded different patterns of global connectivity across states of consciousness, with AEC showing the strongest network connectivity during the *Unconscious* epoch, and wPLI showing the strongest connectivity during full consciousness (i.e., *Baseline* and *Recovery*). Both measures also demonstrated differential predictive contributions across participants and used different brain regions for classification. AEC showed higher classification accuracy overall, particularly for distinguishing anesthetic-induced unconsciousness from *Baseline* (83.7 ± 0.8%). AEC also

showed stronger classification accuracy than wPLI when distinguishing *Unconscious* from *Pre-ROC* (i.e., "deep" from "light" unconsciousness) (AEC: 66.3 ± 1.2%; wPLI: 56.2 ± 1.3%), and when distinguishing between responsiveness and unresponsiveness (AEC: 76.0 ± 1.3%; wPLI: 63.6 ± 1.8%). Classification accuracy was not improved compared to AEC when both AEC and wPLI were combined. This analysis of source-localized EEG data demonstrates that envelope- and phase-based FC provide different information about states of consciousness but that, on a group level, AEC is better able to detect relative alterations in brain FC across levels of anesthetic-induced unconsciousness compared to wPLI.

1. Introduction

The application of network neuroscience to non-invasive brain imaging techniques has broadened our understanding of the anatomical and functional brain architecture that underpins conscious experience. A large sub-domain of these advances has been driven by functional connectivity (FC) and graph theory measures applied to functional neuroimaging (e.g. fMRI) and neurophysiological datasets (e.g. EEG, MEG). As opposed to fMRI-based connectome studies, which assess the statistical dependency of signal amplitudes, studies reconstructing the brain connectome using neurophysiological data have used two modes of intrinsic coupling: envelope coupling (also referred to as amplitude coupling), which probes the temporal relationship between the frequency envelope of two signals, and phase coupling, which measures the phase coherence between two signals (Engel et al., 2013; Sadaghiani and Wirsich, 2020). These distinct coupling modes seem to differ in their spectral and spatial signatures, dynamics, mechanisms, and functions (Engel et al., 2013).

Assessing the amplitude envelope of brain signals has been used to probe long-range temporal correlations (LRTC) in the brains of healthy individuals across various frequency bands (Linkenkaer-Hansen et al., 2004; Nikulin and Brismar, 2004, 2005; Berthouze et al., 2010; Fedele et al., 2016), but has also shown pathological alterations of LRTC in psychiatric disorders, Alzheimer's disease, and epilepsy (Linkenkaer-Hansen et al., 2005; Monto et al., 2007; Slezin et al., 2007; Montez et al., 2009; Bornas et al., 2015). In the context of consciousness research, a recent study found that sevoflurane-induced unconsciousness was associated with increased LRTC in the beta bandwidth in frontocentral regions (Thiery et al., 2018). Combining beta LRTC with alpha amplitude over occipital electrodes classified the state of consciousness versus unconsciousness with an accuracy of 80%.

Phase-coupling modes have also been used to characterize different states of consciousness, or predict recovery. Chennu and colleagues characterized the changes in the alpha-band network constructed with the debiased weighted phase lag index (dwPLI) in unresponsive wakefulness syndrome (UWS) and minimally conscious state (MCS), when compared to healthy subjects (Chennu et al., 2014), and highlighted the diagnostic value of dwPLI for distinguishing UWS from MCS (Chennu et al., 2017). Recently, Kustermann et al. (2020) showed that in the first 24 h following coma due to cardiac arrest, graph theoretical properties (i.e., clustering coefficient, modularity and path length) of the functional network constructed using the dwPLI are associated with long-term outcome. Other studies have showed changes in connectivity induced by pharmacological sedatives (Blain-Moraes et al., 2016, 2017; Li et al., 2019; Ranft et al., 2016; Sripad et al., 2020; Vlisides et al., 2019). Studies comparing sleep to wakefulness or anesthesia have also shown that phase-based coupling can detect region- and frequency-specific changes in connectivity across consciousness states, and may deepen our understanding of the neural correlates of consciousness (Mikulan et al., 2018; Imperatori et al., 2019; Banks et al., 2020; Imperatori et al., 2020).

Although patterns of FC across the brain may provide powerful insight into the neural correlates of consciousness, envelope- and phase-coupling modes have been studied– for the most part – in a mutually exclusive way. Furthermore, task-based connectivity studies have relied heavily on phase-coupling measures, while resting state connectivity studies have used envelope-coupling with increasing prevalence, creating a disconnect in the scientific literature bearing on neurophysiological FC (Sadaghiani and Wirsich, 2020). As a result, a lack of consensus persists around which coupling mode is best suited for identifying the neural correlates of consciousness. Therefore, this study aims to compare two commonly-used FC metrics – an envelope-based measure (i.e. amplitude envelope correlation, or AEC) and a phase-based measure (i.e. wPLI) – in their classification of different states of consciousness derived from the same set of source-localized data across anesthetic-induced alterations of consciousness. Since envelope- and phase-coupling are thought to potentially correspond to distinct modes of information integration within the brain (Engel et al., 2013), we hypothesized that these metrics would draw from different brain regions in their classification of consciousness, and would perform differently in the classification of 1) different consciousness states before, during and after anesthesia, 2) varying depths of anesthetic-induced unconsciousness (light vs. deep), and 3) responsive and unresponsive states.

2. Material and methods

This study is a subset of the Reconstructing Consciousness and Cognition (ReCCognition) study (NCT01911195), conducted at the University of Michigan Medical School and approved by the Institutional Review Board (HUM0071578). All participants provided written informed consent prior to the onset of the experiment. The full protocol can be found in a previous publication (Maier et al., 2017).

2.1. Study population

This study included 9 healthy volunteers (5 men; 24.4 ± 1.0 years old), a subset of the ReCCognition study (Maier et al., 2017) recruited at the University of Michigan. All participants were considered class 1 or 2 physical status by the American Society of Anesthesiologists, had a body mass index below 30, an airway classification of a Mallampati 1 or 2, and no other factors predictive of difficult airways for anesthetic administration. The following criteria excluded volunteers from participating: pregnancy, reactive airway disease, gastroesophageal reflux, cardiac conduction abnormalities, asthma, epilepsy, a history of obstructive sleep apnea, neurologic or psychiatric disorders, family history of issues with anesthesia, and any current or past use of psychotropic medications. Urine and blood samples confirmed that all participants were not currently pregnant and/or using illicit drugs.

2.2. Anesthetic protocol

At least two fully trained anesthesiologists were present throughout the anesthetic protocol. Participants were pre-oxygenated with a face mask and received intravenous infusions of propofol in increasing amounts over three 5-minute periods for slow anesthetic induction (100 μg/kg/min, 200 μg/kg/min, and 300 μg/kg/min, respectively). After the 15-minute administration of propofol, participants were administered isoflurane at age-adjusted 1.3 minimum alveolar concentration via laryngeal mask inhalation for 3 h. To maintain arterial pressure, phenylephrine was titrated as needed. Thirty-minutes prior to ceasing isoflurane, 4 mg of ondansetron was administered to prevent nausea.

Throughout the experiment, participants' motor responsiveness was assessed with an auditory loop instructing them to squeeze their
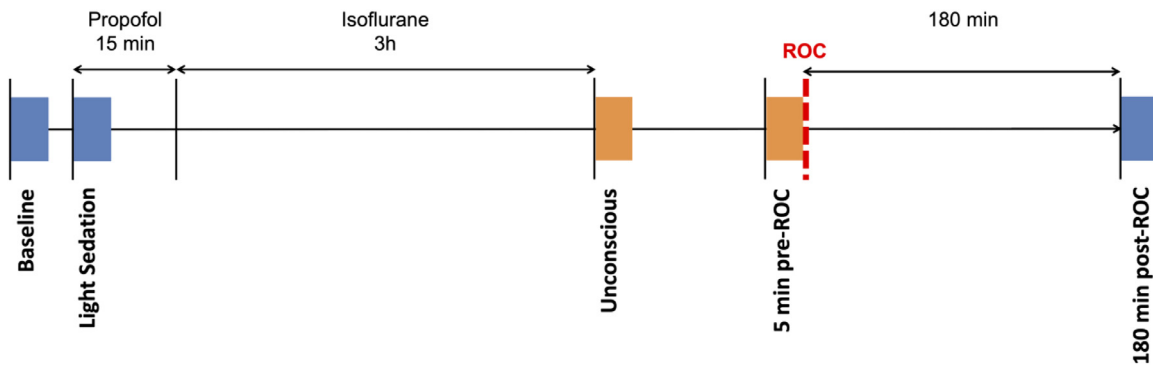
Fig. 1. Experimental design
Timeline of anesthetic protocol and EEG data epochs. Rectangles represent the five 5-min EEG epochs from which functional networks were constructed using an envelope- and a phase-based measure of functional connectivity. Blue rectangles represent epochs of responsiveness, while orange rectangles represent epochs of unresponsiveness. (For interpretation of the references to colour in this figure legend, the reader is referred to the web version of this article.)

left/right hand twice, every 30 s, with the right and left command randomized, as in previous studies (Purdon et al., 2013; Blain-Moraes et al., 2015, 2017; Vlisides et al., 2017; Kim et al., 2018; Thiery et al., 2018; Nadin et al., 2020; Duclos et al., 2021). Loss of consciousness (LOC) was estimated through loss of responsiveness, which was defined as the first time that a subject failed to respond to two consecutive commands. Recovery of consciousness (ROC) was estimated through return of responsiveness, which was defined as the earliest instance in which participants correctly responded to two consecutive audio loop commands.

2.3. Data acquisition and preprocessing

EEG data were acquired at 500 Hz with gel-based electrodes using a 128-channel amplifier from Electrical Geodesics, Inc. (Eugene, OR) during the entire duration of the anesthetic protocol. All channels were referenced to the vertex (Cz). Immediately prior to the start of EEG data collection, electrode impedances were reduced to below 50 kΩ.

Upon completion, data were preprocessed in EEGlab. The signal was average referenced, down-sampled to 250 Hz, and visually inspected to manually reject noisy channels and signal sections containing large artifacts. Some subjects and experimental states were therefore left with cleaned data segments slightly shorter than 5 min. When data segments were removed, data were re-joined (i.e., concatenated) at the boundary (see Supplementary Materials for a complete list of the duration of cleaned data segments and number of boundaries, per participant and experimental state). Previous studies have shown evidence for changes in the alpha bandwidth under anesthetic-induced unconsciousness (Ching et al., 2010; Lee et al., 2013a, 2013b; Purdon et al., 2013; Blain-Moraes et al., 2014, 2017; Mukamel et al., 2014). Based on this evidence, we decided to investigate the alpha frequency band in the recent study and bandpass-filtered the signal in from 8 to 13 Hz.

During the experiment, five minutes of continuous EEG was recorded in five experimental states, some of which reflect transitions in and out of anesthetic-induced consciousness (Fig. 1). The (1) *Baseline* recording took place prior to any anesthetic administration; (2) *Light Sedation:* the first 5 min of propofol administration at a steady infusion rate of 100 μg/kg/min, during which participants were behaviorally responsive; (3) *Unconscious:* the first 5 min after the discontinuation of all anesthetics (i.e., the end of the 3-hour period of anesthesia at surgical level), during which all participants remained unresponsive but the brain was beginning its transition toward the recovery of consciousness; (4) *Pre-ROC:* the last 5-minute period of unresponsiveness, immediately prior to the ROC, reflecting the end of the brain's transition toward the recovery of consciousness; and the (5) *Recovery* recording, which took place 180 min following ROC. During all experimental states, partic-

ipants were instructed to remain still with their eyes closed. For the purpose of this study, we selected the first five minutes of continuous EEG data from each state.

2.4. Electroencephalography analysis

2.4.1. Source estimation

Preprocessed EEG data were imported into the Brainstorm analysis software for source estimation (Tadel et al., 2011). The brain volume current source-density mapping was calculated with a distributed model containing 45,000 dipoles (oriented in 3 directions across 15,000 vertices), with the dipole orientations unconstrained. The brain model of the Montreal Neurological Institute served as the brain anatomy for all participants. This brain model was then warped to the geometry of our sensor net (GSN HydroCel 128). The forward model, computed with a Symmetric Boundary Element Method, was computed in Brainstorm using the open-source software OpenMEEG (Gramfort et al., 2010; Kybic et al., 2005). All analysis epochs were used to generate a data covariance matrix, while the identity matrix was used as the noise covariance matrix.

Linearly constrained minimum variance (LCMV) beamformers were used to estimate the source activity, Pseudo Neural Activity Index (PNAI), at each defined location within Brainstorm (Tadel et al., 2011). The median eigenvalue was used to regularize the data covariance matrix. Finally, the mean source activity at each ROI (i.e., the mean of all voxels within each ROI), as defined by the Automated Anatomical Labeling (AAL) Atlas, was extracted to generate a single time series for 82 defined cortical ROIs across all participants.

The confound of signal leakage (i.e., the non-independence of voxels in source space) was mitigated using pairwise orthogonalization, a multivariate approach that assesses power-power interaction between oscillations extracted for spatially separate ROIs (Brookes et al., 2012), applied to each 10-second window. In this technique, signal leakage between voxels is expected to affect all frequency components equally. Signal leakage between X and Y was removed by reshaping these matrices into vectors x and y, from which a univariate projection was estimated:

$$\beta_{UV} = \mathbf{x}^+\mathbf{y}$$

where $\mathbf{x}^+$ denotes the pseudo-inverse of x. The estimate of y based on vector x is removed thus:

$$\mathbf{y_R} = \mathbf{y} - \mathbf{x}\beta_{UV}$$

where y_R is the component of y that is orthogonal to x. As such, any linear interaction between x and y was removed.

2.4.2. Envelope-based connectivity: amplitude envelope correlation

Amplitude envelopes were generated via a Hilbert transform of the source-localized EEG in 10-second epochs, across all participants and experimental states. Pearson correlations were then computed between all amplitude envelopes across all combinations of ROI pairs, resulting in an 82×82 Amplitude Envelope Correlation (AEC) for each 10-second epoch. To calculate the AEC over each experimental state, the 10-second window was shifted over the whole signal with a step size of one second. To visualize the AEC matrix for each experimental state, the AEC was averaged over all individuals and states. Global connectivity of AEC was calculated as the mean connectivity of each ROI to the rest of the brain regions defined in the AAL atlas, and was calculated for each experimental state.

2.4.3. Phase-based connectivity: weighted phase lag index

The wPLI (Vinck et al., 2011) is defined by the phase difference between two signals s_i and s_j, weighted by the magnitude of the imaginary component of the cross-spectrum $\mathcal{J}(C_{ij})$ and was calculated using the following function:

$$wPLI_{ij} = \frac{\left| E\{\mathcal{J}(C_{ij})\} \right|}{E\left\{ \left| \mathcal{J}(C_{ij}) \right| \right\}} = \frac{\left| E\left\{ \left| \mathcal{J}(C_{ij}) \right| sgn(\mathcal{J}(C_{ij})) \right\} \right|}{E\left\{ \left| \mathcal{J}(C_{ij}) \right| \right\}}$$

where E{.} denotes the expected value operator and sgn(.) refers to the sign function (Vinck et al., 2011). The wPLI takes on values of $0 \leq$ wPLI ≤ 1, with 1 indicating a strong functional coupling relationship and 0 indicating no connectivity. Similar to AEC, wPLI was calculated in 10-second epochs with a step size of one second across each 5-minute state, resulting in one time-series of FC matrices for each experimental state. Global connectivity of wPLI was calculated as the mean connectivity of each ROI to the rest of the brain regions defined in the AAL atlas, and was calculated for each experimental state.

2.5. Machine learning analysis

We implemented a machine learning (ML) framework for epoch-by-epoch classification of the five states of consciousness (i.e., *Baseline, Light Sedation, Unconscious, Pre-ROC, Recovery*) using features of the AEC and wPLI FC matrices. The complete machine learning pipeline was implemented using scikit-learn.

2.5.1. Feature extraction

Each experimental state in this study consisted of a FC time-series, with each epoch containing the AEC or wPLI connectivity over a 10-second window. To provide meaningful features to the machine learning models, each epoch was characterized by the overall connectivity of all ROIs to the whole brain (i.e., the mean and standard deviation across all columns of the AEC and wPLI connectivity matrices). The features of each epoch (i.e., mean and standard deviation for each ROI) were normalized across all participants using a min-max feature scaling normalization. Across all experimental states, this formed an observation space (i.e. total number of 10-second epochs on which FC was calculated) of $n = 12{,}816$ (*Baseline* = 2472 epochs; *Light Sedation* = 2603 epochs; *Unconscious* = 2619 epochs; *Pre-ROC* = 2603 epochs; *Recovery* = 2523 epochs) (see Supplementary Materials for a detailed list of the observation space per participant and experimental state). Given that AEC and wPLI were calculated on the same data, the observation space was identical for both metrics.

2.5.2. Model selection

To identify the machine learning model which best distinguished between *Baseline* and pharmacologically induced unconsciousness, we implemented two different binary classifiers independently targeting *Baseline* vs. *Unconscious* and *Pre-ROC*. Several classification techniques were initially tested for the binary classifiers, including linear-discriminant

analysis (LDA), linear kernel support vector machine (SVM$_{linear}$) and radial basis function kernel support vector machine (SVM$_{radial}$). For both support vector machines, we conducted a parameter sweep of regularization parameter C. To account for the high degree of correlation between epochs collected from a single participant, each binary classifier was implemented using a leave-one-subject-out (LOSO) cross-validation, completely excluding the participant being tested from the training set. Each binary classifier was trained on three sets of data: 1) AEC features alone; 2) wPLI features alone; and 3) wPLI and AEC features combined. Each model's overall accuracy was determined by the average accuracy over all 9 LOSO repetitions. For the remainder of the analysis, we selected the model which achieved the highest accuracy to distinguish *Baseline* from *Unconscious* and *Pre-ROC* over the different sets of data.

2.5.3. Classification

To investigate the contribution of AEC and wPLI FC for distinguishing *Baseline* and other experimental states (i.e. *Light Sedation, Unconscious, Pre-ROC* and *Recovery*), four different classifiers were implemented with the previously selected parameters. We trained two additional classification models: one for distinguishing between *Unconscious* ("deep" unconsciousness) and *Pre-ROC* ("light" unconsciousness); another for distinguishing between responsiveness (*Baseline, Light Sedation,* and *Recovery*) and unresponsiveness (*Unconscious* and *Pre-ROC*). All six classifiers were trained individually on three sets of data: 1) AEC features alone; 2) wPLI features alone; and 3) wPLI and AEC features combined. Additionally, all models were implemented using LOSO cross-validation. Each model's performance was evaluated by the average over all 9 LOSO repetitions.

The contribution of each feature towards classifier performance was assessed according to their relative weights in the fully trained linear SVM. The absolute value of the weights was then min-max normalized to obtain a relative feature importance per classifier. We then generated a brain map highlighting the participation of ROIs in the classification, according to feature mean, standard deviation or both.

2.5.4. Statistical analysis

The statistical significance of the classifier performance was assessed using permutation testing. Within the permutation testing, classifier performance was evaluated using a LOSO cross-validation. The labels of the training and test data were randomly permuted and classification accuracy was assessed with the permuted dataset. This process was repeated 10,000 times to create a null distribution of random accuracy. Accuracy of the true classifier was deemed significant at $p < 0.001$ if it was greater than all 10,000 permutation accuracies.

2.5.5. Comparison between classifiers

The relative discriminatory information of states of consciousness provided by AEC vs. wPLI connectivity was assessed by generating bootstrap confidence intervals for each classifier. The bootstrap dataset was created by sampling with replacement from the original dataset until a new dataset (containing duplicate samples) of the same size was generated. The bootstrap dataset was separated into training and test sets, and used to characterize the performance of the SVM$_{linear}$. This process was repeated 10,000 times, creating a distribution of the classifier performance. Lower and upper bounds for the bootstrap confidence interval were set at the 2.5th and 97.5th percentile, corresponding to $p \leq 0.05$. Two classifiers were considered to have statistically different levels of performance if their confidence interval did not overlap with a bootstrap resampling of 500.

3. Results

3.1. Envelope- and phase-based connectivity measures yield different patterns of global connectivity across states of consciousness

Connectivity patterns, and the brain regions involved in global connectivity, varied between envelope- and phase-based measures of FC
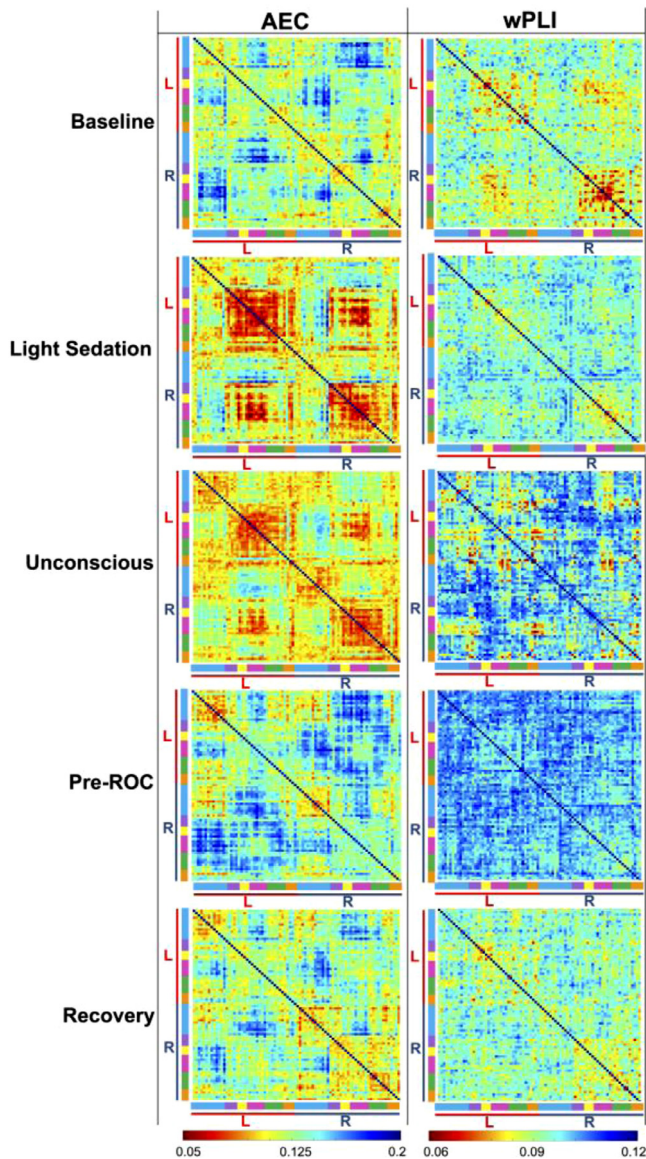
Fig. 2. Average connectivity matrixes in the alpha band between the 82 cortical regions of interest across states of consciousness

Connectivity matrices averaged over all participants, for each experimental state and for each measure (i.e. Amplitude Envelope Correlation (AEC) and weighted Phase Lag Index (wPLI)). Red represents higher strength in connectivity, while blue represents lower strength in connectivity. Both right (R) and left (L) hemispheres are depicted in each matrix.

(Fig. 2, Fig. 3). While AEC yielded the strongest network connectivity during the *Unconscious* epoch, wPLI connectivity was strongest during full consciousness (i.e. *Baseline* and *Recovery*).

AEC: During full consciousness (i.e. *Baseline* and *Recovery*), AEC showed weak connectivity overall, with the strongest connectivity located in the central and temporal regions. *Light Sedation* was marked by a pronounced increase in connectivity in parietal and occipital regions, which was then further amplified during the *Unconscious* state, showing increased connectivity across the brain. *Pre-ROC* was characterized by an overall decrease in connectivity, most prominent in the parietal, temporal and occipital regions.

wPLI: During full consciousness (i.e. *Baseline* and *Recovery*), wPLI showed the strongest connectivity in the temporal, parietal and occipital regions. During *Light Sedation*, there was a slight global decrease in connectivity, with the occipital regions remaining most strongly con-
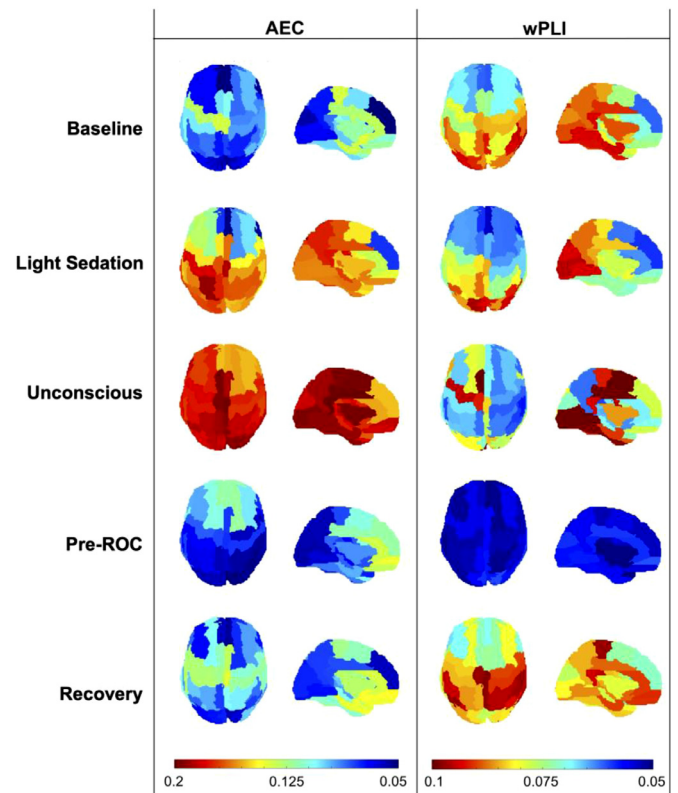

Fig. 3. Topographic maps of source-localized global connectivity in the alpha band between the 82 cortical regions of interest across states of consciousness. To compare and contrast the patterns of connectivity captured by Amplitude Envelope Correlation (AEC) and weighted Phase Lag Index (wPLI) across various states of consciousness, the group-level means of AEC and wPLI for each 5-minute epoch were displayed on 82 regions of a brain parcellated according to the AAL atlas. For each time point and for each measure, the same topographic map is depicted in 2 different views: axial top view (left), and mid-sagittal view of the left hemisphere (right). The average connectivity of each ROI to the rest of the brain regions defined in the AAL atlas is depicted by a color: red represents higher strength in connectivity, while blue represents lower strength in connectivity.

nected. The *Unconscious* epoch was marked by an increase in frontal and central connectivity in the left hemisphere and along the midline and inferior temporal gyrus. Of all experimental states, *Pre-ROC* showed the weakest connectivity in all ROIs.

Inter-hemispheric differences in ROI connectivity strength were present across all states, for both AEC and wPLI.

3.2. AEC shows superior classification accuracy to wPLI across states of anesthetic-induced unconsciousness

The SVM_{linear} with $C = 0.1$ yielded the highest classifier performance and was therefore used for all analyses in this study.

3.2.1. Differences in classification accuracy across states of consciousness

Globally, AEC performed better than wPLI in the classification of the different states of consciousness, when comparing these states to *Baseline* (Fig. 3A). Highest accuracy for AEC was found in the classification of the *Unconscious* state (83.7 ± 0.8% [95% CI: 82.0–85.5%]), followed by *Pre-ROC* (68.5 ± 1.0% [95% CI: 66.6–70.4%]), *Light Sedation* (54.0 ± 1.4% [95% CI: 50.9–56.5%]), and *Recovery* (52.8 ± 1.4% [95% CI: 49.9–55.3%]). Though the classification accuracies of *Light Sedation* and *Recovery* were close to chance, permutation analysis revealed that all classification accuracies were statistically higher than chance in distinguishing them from *Baseline* ($p < 0.001$).
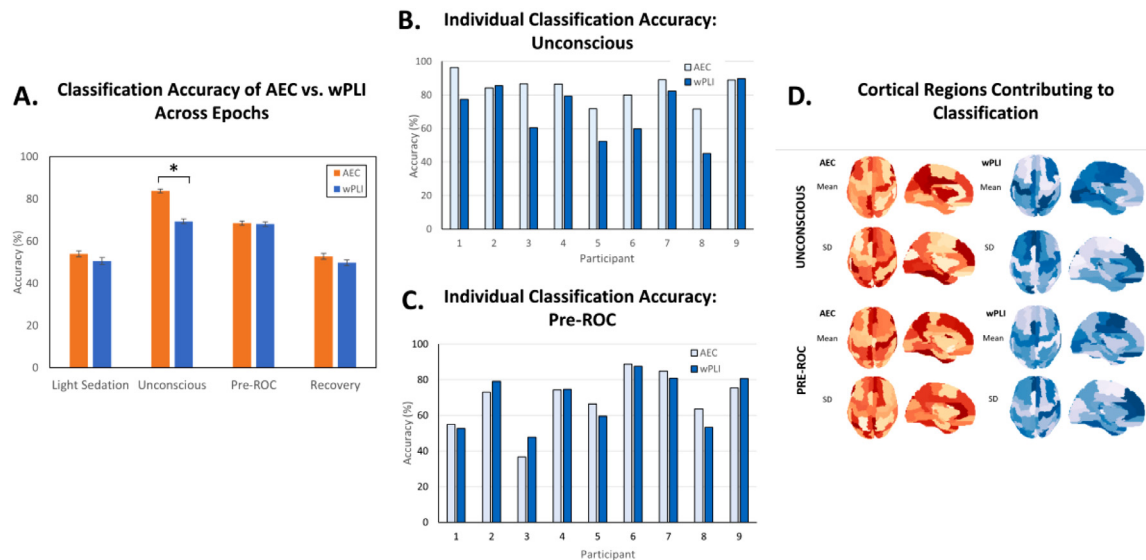
Fig. 4. AEC vs. wPLI classification of states of consciousness

Machine learning results comparing classification accuracy across connectivity measures (A) and individuals (B, C): A) Classification accuracies of Amplitude Envelope Correlation (AEC) and weighted Phase Lag Index (wPLI) for the *Light Sedation, Unconscious, Pre-ROC* and *Recovery* epochs; B) Individual classification accuracies for the *Unconscious* epoch, for both AEC (light blue) and wPLI (dark blue); C) Individual classification accuracies for the *Pre-ROC* epoch, for both AEC (light blue) and wPLI (dark blue); D) Implication of the various cortical regions of interest in the classification of the *Unconscious* and *Pre-ROC* epochs by AEC (red) and wPLI (blue), according to feature mean (top) and standard deviation (bottom). The axial top view and mid-sagittal view of the left hemisphere are depicted. (For interpretation of the references to colour in this figure legend, the reader is referred to the web version of this article.)

For wPLI, the classification accuracy of the *Unconscious* state was statistically lower than that of AEC, while other classification accuracies did not differ statistically from that of AEC. Specifically, wPLI classification accuracies were highest for the *Unconscious* state (69.4 ± 1.1% [95% CI: 67.3–71.7%]), followed by *Pre-ROC* (68.1 ± 1.1% [95% CI: 65.9–70.1%]), *Light Sedation* (50.6 ± 1.6% [95% CI: 47.3–54.0%]), and *Recovery* (49.8 ± 1.4% [95% CI: 47.1–52.4%]). Permutation analysis revealed that wPLI accuracies were no higher than chance at both *Light Sedation* and *Recovery*, which are both states where responsiveness is present.

Though AEC had significantly higher classification accuracy for *Unconsciousness* than for *Pre-ROC* ($p < 0.05$), wPLI did not show a significant difference in classification accuracies between these states. When combining both AEC and wPLI, classification accuracies were not statistically improved for any time point, when compared to AEC classification accuracies: *Unconscious* (84.1 ± 0.9% [95% CI: 82.5–85.8%]), *Pre-ROC* (69.8 ± 1.0% [95% CI: 67.8–71.7%]), *Light Sedation* (52.6 ± 1.3% [95% CI: 50.0–55.0%]), and *Recovery* (54.6 ± 1.4% [95% CI: 51.8–57.4%]). This suggests that AEC independently performed as well as AEC combined with wPLI.

3.2.2. Inter-individual differences in the classification accuracy of states of consciousness

As shown in Figs. 4B and 4C, there were high inter- and intra-individual differences in the classification accuracies of AEC and wPLI. For the *Unconscious* state, inter-individual classification accuracies for AEC ranged from 71.6% to 96.4%, while they varied between 45.1% and 89.7% for wPLI. For *Pre-ROC,* classification accuracy values ranged from 36.8% to 88.7% for AEC and between 47.7% and 87.6% for wPLI. Intra-individual differences in classification accuracies were also highly variable. Within a single individual, the difference in the classification accuracy between wPLI and AEC reached up to 26.2% for the *Unconscious* state, and up to 10.9% for *Pre-ROC*.

3.2.3. Differences in the brain regions contributing to classification accuracy of consciousness states

The brain regions most involved in the classification of *Unconscious* and *Pre-ROC* varied between AEC and wPLI (Fig. 5B). Both the normalized means and standard deviations contributed to the classification of consciousness states. During *Unconscious*, the brain regions most involved in classification with AEC were fairly dispersed throughout the brain, while those implicated in the classification with wPLI connectivity were mainly located posteriorly when they contributed with their mean, or anteriorly when they contributed with their standard deviation. During *Pre-ROC*, the ROIs most involved in the classification with AEC were also dispersed throughout the brain. Conversely, those implicated in the classification with wPLI were mainly located in posterior regions when they contributed with their mean, or in the frontal, temporal and parietal regions when they contributed to the classification with their standard deviation. In both cases, there were important interhemispheric differences in the weight of each ROI's contribution to the classification. This was particularly apparent for AEC, whose classification accuracy depended more heavily on the right hemisphere, particularly for frontal and central ROIs. Although both metrics predicted the same state, using the same signal, these results suggest that they draw from different regions of the brain in the classification of states of consciousness.

3.3. AEC is better able to distinguish different depths of unconsciousness than wPLI

In the classification model aiming to distinguish *Unconscious* ("deep" unconsciousness) from *Pre-ROC* ("light" unconsciousness), AEC was better able to distinguish different depths of unconsciousness than wPLI (Fig. 5A). More specifically, the model aiming to distinguish *Unconscious* from *Pre-ROC* yielded a classification accuracy of 66.3 ± 1.2% [95% CI: 64.1–68.8%] for AEC, which was statistically higher than the 56.2 ± 1.3% [95% CI: 53.8–58.8%] accuracy attained with wPLI ($p < 0.05$). Combing both AEC and wPLI did not further improve classification accuracy when compared to AEC alone, as the model combin-
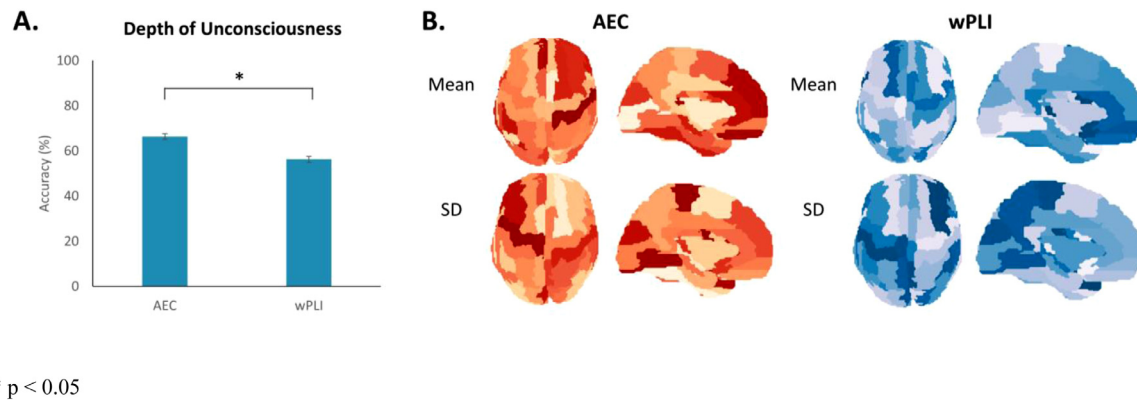
Fig. 5. AEC vs. wPLI classification of "deep" vs. "light" unconsciousness

A: Classification accuracies of Amplitude Envelope Correlation (AEC) and weighted Phase Lag Index (wPLI) in a model that distinguishes *Unconscious* ("deep" unconsciousness) from *Pre-ROC* ("light" unconsciousness). B: Degree of implication of the various cortical regions of interest in the classification of the *Unconscious* and *Pre-ROC* epochs by AEC (red) and wPLI (blue), according to feature mean (top), standard deviation (bottom). The axial top view and mid-sagittal view of the left hemisphere are depicted.

[*] $p < 0.05$. (For interpretation of the references to colour in this figure legend, the reader is referred to the web version of this article.)
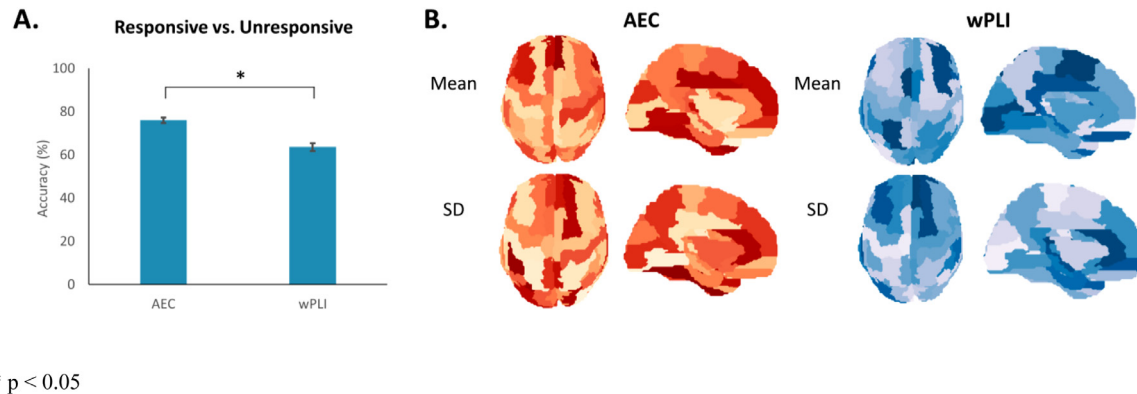

Fig. 6. AEC vs. wPLI classification of responsiveness vs. unresponsiveness

A: Classification accuracies of Amplitude Envelope Correlation (AEC) and weighted Phase Lag Index (wPLI) in a model that distinguishes responsiveness (i.e. *Baseline, Light Sedation, Recovery*) from unresponsiveness (i.e. *Unconscious, Pre-ROC*). B: Degree of implication of the various cortical regions of interest in the classification of responsiveness and unresponsiveness, by AEC (red) and wPLI (blue), according to feature mean (top) and standard deviation (bottom). The axial top view and mid-sagittal view of the left hemisphere are depicted.

[*] $p < 0.05$. (For interpretation of the references to colour in this figure legend, the reader is referred to the web version of this article.)

ing AEC and wPLI yielded an accuracy of 66.4 ± 1.2% [95% CI: 64.2–68.8%].

The brain regions most involved in the classification of *Unconscious* vs. *Pre-ROC* varied between AEC and wPLI (Fig. 5B). For this model, the brain regions involved in the classification with AEC were fairly dispersed throughout the brain and had marked differences between hemispheres. While the ROIs implicated in the classification with wPLI also showed hemispheric differences, ROIs contributing to the classification with their mean were mainly located centrally and posteriorly, and those contributing with their standard deviation were primarily anterior.

3.4. AEC is better able to distinguish responsive from unresponsive states than wPLI

In the classification model aiming to distinguish responsive (i.e. *Baseline, Light Sedation, Recovery*) from unresponsive states (*Unconscious, Pre-ROC*), AEC was better able to distinguish responsiveness from unresponsiveness than wPLI (Fig. 6A). More specifically, this model yielded a statistically higher classification accuracy for AEC (76.0 ± 1.3% [95% CI: 73.5–78.2%]) than for wPLI (63.6 ± 1.8% [95% CI: 59.7–66.7%]) ($p < 0.05$). Combing both AEC and wPLI did not further improve classification accuracy when compared to AEC alone, as the model combin-

ing AEC and wPLI yielded an accuracy of 73.6 ± 1.4% [95% CI: 70.9–76.1%].

The brain regions most involved in the classification of responsive vs. unresponsive states also varied between AEC and wPLI (Fig. 6B). The brain regions most involved in classification with AEC were fairly dispersed throughout the brain, while those implicated in the classification with wPLI were mainly located posteriorly when they contributed with their mean, or anteriorly when they contributed with their standard deviation, though not exclusively so.

4. Discussion

In this study, we directly compared source-localized brain networks constructed from envelope-based and phase-based FC metrics, the AEC and wPLI, using the same EEG dataset collected across multiple states of anesthetic-induced unconsciousness. We found that global alpha connectivity patterns associated with various states of consciousness were distinct when constructed with AEC or wPLI. These two FC metrics had varying degrees of predictive power in different states of unconsciousness, yielded important inter-individual differences in predictive power, and drew from different brain regions in their classification of states of consciousness. Importantly, on the group level, AEC had higher classi-

fication accuracy than wPLI across states of consciousness, in distinguishing deep from light unconsciousness (*Unconscious* vs. *Pre-ROC)*, and in distinguishing responsive from unresponsive epochs. Our results suggest that AEC and wPLI construct distinct functional networks and differentially characterize the brain's functional reorganization across changes in states of consciousness. However, the envelope-based metric AEC emerges as the superior metric of the two in contrasting changes in states of consciousness and responsiveness.

The results of our study are concordant with the handful of studies published to-date that contrast envelope- and phase-based coupling in the brain. In support of our findings, a few such studies have also concluded that AEC is more robust than various phase-based measures. Colclough et al. (2016) compared the repeatability and reproducibility of various envelope- and phase-coupling measures using MEG, and concluded that AEC was the most consistent and reproducible, while poor test-retest reliability was found in PLI (phase-based) and the imaginary part of coherency (envelope-based). Another study also confirmed the higher reproducibility of AEC in Alzheimer's disease for alpha-band connectivity, when compared to phase-based measured including PLI (Briels et al., 2020). While our study is the first to compare these metrics across states of consciousness, other studies have also shown that the two classes of connectivity differentially characterize brain function, as they most likely underpin distinct cortical processes. Helfrich et al. (2016) investigated the processing of visual sensory input using both envelope- and phase-coupling in the gamma frequency band. Globally, they concluded that the two coupling modes sustained different cortical processes involved in conscious perception of a moving stimulus. Guggisberg et al. (2015) came to a similar conclusion when they compared AEC and lagged phase synchronization of resting-state alpha and beta frequencies. The authors found a significant interaction between coupling mode and frequency, as well as between coupling mode and spatial interaction pattern. More specifically, they found that their phase-based measure was associated with global network interactions, while their envelope-based measure was associated with local and intra-hemispheric connections, leading them to conclude that phase- and envelope-coupling provide complementary information about brain function. The complementary roles of phase- and envelope-based coupling have also been demonstrated in intracranial EEG, where they have been shown to exhibit divergent properties in their time-varying response to an external stimulus (Mostame et al., 2019).

It is worth highlighting that while the overall classification results were higher for AEC, there are significant individual differences in the predictive power of each type of FC metric. For some (e.g. participant 4), networks constructed from wPLI are more predictive of both states of unconsciousness. While this variability may be explained by the inter-individual systematic differences in whole-brain resting FC (Finn et al., 2015), we posit that both types of connectivity may play a functional role in maintaining a state of criticality in brain networks. The criticality phenomenon in neuronal networks implies that the system is at a metastable state with a delicate balance between excitation and inhibition (Shew and Plenz, 2013). Phase-based measures have been able to distinguish the distance from criticality in both pharmacologically and pathologically disturbed states of consciousness (Lee et al., 2018). Similarly, envelope-based measures such as LRTC have shown changes in states of consciousness associated with imbalance between excitation and inhibition in neuronal networks, resulting in a loss of dynamic range (Shew et al., 2009), information transfer and information capacity (Larremore et al., 2011). The networks with the greatest predictive power for conscious state for any given individual are likely to be constructed from the class of FC that best reflects the distance of that individual's brain from critical dynamics. As the classifiers in the present study were not designed for individual classification of consciousness states, future consciousness studies assessing FC on a single-subject level should consider investigating multiple coupling modes to determine which metric is best suited to identify consciousness alterations within the individual.

The results of this study should be interpreted within the context of several strengths. First, we used connectivity measures derived from a high-density EEG dataset recorded from a clinically-realistic anesthetic regimen. Second, we validated our source-localized resting state FC patterns against those generated in a MEG-based study (Brookes et al., 2011). Our ability to reproduce these baseline FC patterns lends credibility to our FC analysis. Third, our results are classifier agnostic. While we only report classification accuracy of the highest-performing classifier (e.g. linear SVM), we obtain similar patterns with LDA and nonlinear SVM classifiers, lending credibility to our ML analysis. Fourth, our results are robust across different brain atlases. While we only report FC and ML results generated from the AAL atlas, we reproduced our functional connectivity analyses using the Desikan-Killiany brain atlas and found similar connectivity patterns. Finally, our results acknowledge that while we have used responsiveness as a surrogate marker for consciousness, these states are not always equivalent (Sanders et al., 2012). We ran two independent analyses comparing the classification of AEC and wPLI across states of consciousness *and* states of responsiveness. In both analyses, the classification accuracy of AEC was superior in comparison to wPLI and the combination of AEC and wPLI, fortifying our results against instances where the two states may be dissociated.

The results also need to be interpreted in light of several limitations. First, the number of participants in the study is relatively low ($n = 9$). We accounted for this limitation by applying a single-epoch machine learning approach, using all data segments segregated across all participants ($n = 5076$), and controlled for biases due to subject idiosyncrasies by applying a LOSO procedure, which ensured that the classifier did not train on the data it was subsequently classifying. Second, we use a single measure of phase-based connectivity (i.e., wPLI) and a single measure of envelope-based connectivity (i.e., AEC) to assess the performance of these classes of functional coupling in the classification of states of consciousness. There is a large selection of other metrics within both classes; our results may be biased by the selection of a metric in the FC class that is not optimal for assessing consciousness. Third, unconsciousness was induced by exposing participants to an anesthetic – it is possible that the changes in connectivity that we observed are a result of the anesthetic drug, rather than the state of (un)consciousness itself. Moreover, different drugs were used for anesthesia induction and maintenance, and could have differing effects on the EEG. Our results need to be confirmed in future studies across varying altered states of consciousness, such as sleep, disorders of consciousness, or general anesthesia with other agents. Fourth, the machine learning algorithms used in this study were selected primarily based on the interpretability of the trained weights; a more complex algorithm with a sufficiently large data set would perform better, however its decision boundary would be difficult to interpret. Fifth, classification accuracy was estimated based on the percentage of correctly labeled time steps within five experimental states. This approach therefore does not account for the temporal variations within each state, which have been shown to reveal rich information about the FC dynamics in altered states of consciousness (Cavanna et al., 2018), including sleep (El-Baba et al., 2019) and pharmacologically induced unconsciousness (Li et al., 2019; Vlisides et al., 2019; Zhang et al., 2019). Furthermore, the *Light Sedation, Unconscious,* and *Pre-ROC* states were likely periods during which effect site concentrations of the anesthetic were gradually changing. Averaging FC metrics over these 5-minute periods therefore prevents the identification of the granular FC changes within these epochs. Sixth, the features for the machine-learning pipeline were defined by the mean and standard deviation across all columns of the AEC and wPLI connectivity matrices (i.e., from one ROI to all other ROIs). Thus, the interpretation of our results is limited to assumptions about the connectivity of one ROI to the whole brain, rather than the connectivity between two distinct ROIs. Further research is needed to investigate FC on a more spatially fine-grained feature space, containing all possible individual connections. Finally, our results apply to varying states of consciousness using source-localized data in the alpha bandwidth, and may not apply to other frequency

bands, paradigms, tasks or states. Future work should assess the relative contribution of envelope- and phase-based FC to other types of brain analysis.

5. Conclusion

The consideration of the type of connectivity to be used in the construction of functional brain networks has significant implications for the study of consciousness. This is the first study to directly compare an envelope- and a phased-based measure of FC across states of consciousness. Using the same source-localized EEG dataset collected across multiple states of anesthetic-induced unconsciousness in healthy adults, this study shows that both AEC and wPLI in the alpha band are distinct in their global connectivity, predictive power, and in the brain regions contributing the highest predictive power. In particular, we showed that AEC performed better than wPLI in the classification of different states of consciousness, when distinguishing different depths of anesthetic-induced unconsciousness, and when distinguishing responsive from unresponsive states. AEC and wPLI showed dissimilar connectivity patterns across states and drew from different brain regions for classification. Overall, our study suggests that the class of connectivity measure chosen to construct functional brain network may greatly influence what connectivity alterations are appraised across states of consciousness, and when these alterations are most apparent. Future FC studies should aim to bridge the methodological gap between envelope- and phase-based coupling modes, and consider expanding their analytic toolset to consider the multi-faceted analysis of waveforms, considering both the envelope and phase, in order optimize the characterization and interpretation of brain functional dynamics.

Data and code availability statements

The data that support the findings of this study are available from the corresponding author, SBM, upon reasonable request.

Code for data analysis is provided as part of the replication package. It is available at for review at https://github.com/BIAPT/AEC-wPLI-comparison.

Author statement

Catherine Duclos: Conceptualization, Methodology, Writing – original draft, Visualization. **Charlotte Maschke:** Methodology, Formal Analysis, Software, Validation, Writing – review & editing. **Yacine Mahdid:** Methodology, Formal Analysis, Software. **Kathleen Berkun**: Methodology, Formal analysis. **Jason da Silva Castanheira**: Formal analysis. **Vijay Tarnal**: Investigation. **Paul Picton**: Investigation. **Giancarlo Vanini**: Investigation. **Goodarz Golmirzaie**: Investigation. **Ellen Janke:** Investigation. **Michael S. Avidan:** Funding acquisition, Conceptualization. **Max B. Kelz:** Funding acquisition, Conceptualization. **Lucrezia Liuzzi**: Methodology, Software, Writing – review & editing. **Matthew J. Brookes**: Methodology, Writing – review & editing. **George A. Mashour**: Funding acquisition, Conceptualization, Writing – review & editing. **Stefanie Blain-Moraes:** Conceptualization, Methodology, Validation, Resources, Writing – review & editing, Visualization, Supervision, Project administration, Funding acquisition.

Funding

Acknowledgements

Supplementary materials

Supplementary material associated with this article can be found, in the online version, at doi:10.1016/j.neuroimage.2021.118169.

References

. . . Banks, M.I., Krause, B.M., Endemann, C.M., Campbell, D.I., Kovach, C.K., Dyken, M.E., Nourski, K.V., 2020. Cortical functional connectivity indexes arousal state during sleep and anesthesia. Neuroimage 211, 116627. doi:10.1016/j.neuroimage.2020.116627.

Berthouze, L., James, L.M., Farmer, S.F., 2010. Human EEG shows long-range temporal correlations of oscillation amplitude in Theta, Alpha and Beta bands across a wide age range. Clin. Neurophysiol. 121 (8), 1187–1197. doi:10.1016/j.clinph.2010.02.163.

. . . Blain-Moraes, S., Boshra, R., Ma, H.K., Mah, R., Ruiter, K., Avidan, M., Mashour, G.A., 2016. Normal brain response to propofol in advance of recovery from unresponsive wakefulness syndrome. Front. Hum. Neurosci. 10, 248. doi:10.3389/fnhum.2016.00248.

Blain-Moraes, S., Lee, U., Ku, S., Noh, G., Mashour, G.A., 2014. Electroencephalographic effects of ketamine on power, cross-frequency coupling, and connectivity in the alpha bandwidth. Front. Syst. Neurosci. 8, 114. doi:10.3389/fnsys.2014.00114.

. . . Blain-Moraes, S., Tarnal, V., Vanini, G., Alexander, A., Rosen, D., Shortal, B., Mashour, G.A., 2015. Neurophysiological correlates of sevoflurane-induced unconsciousness. Anesthesiology 122 (2), 307–316. doi:10.1097/aln.0000000000000482.

. . . Blain-Moraes, S., Tarnal, V., Vanini, G., Bel-Behar, T., Janke, E., Picton, P., Mashour, G.A., 2017. Network efficiency and posterior alpha patterns are markers of recovery from general anesthesia: a high-density electroencephalography study in healthy volunteers. Front. Hum. Neurosci. 11, 328. doi:10.3389/fnhum.2017.00328.

Bornas, X., Fiol-Veny, A., Balle, M., Morillas-Romero, A., Tortella-Feliu, M., 2015. Long range temporal correlations in EEG oscillations of subclinically depressed individuals: their association with brooding and suppression. Cogn. Neurodyn. 9 (1), 53–62. doi:10.1007/s11571-014-9313-1.

Brookes, M.J., Woolrich, M., Luckhoo, H., Price, D., Hale, J.R., Stephenson, M.C., Barnes, G.R., Smith, S.M., Morris, P.G, 2011. Investigating the electrophysiological basis of resting state networks using magnetoencephalography. Proc. Natl. Acad. Sci. 108 (40), 16783–16788. doi:10.1073/pnas.1112685108.

Brookes, M.J., Woolrich, M.W., Barnes, G.R., 2012. Measuring functional connectivity in MEG: a multivariate approach insensitive to linear source leakage. Neuroimage 63 (2), 910–920. doi:10.1016/j.neuroimage.2012.03.048.

Briels, C.T., Schoonhoven, D.N., Stam, C.J., de Waal, H., Scheltens, P., Gouw, A.A., 2020. Reproducibility of EEG functional connectivity in Alzheimer's disease. Alzheimers Res. Ther. 12 (1), 68. doi:10.1186/s13195-020-00632-3.

Cavanna, F., Vilas, M.G., Palmucci, M., Tagliazucchi, E., 2018. Dynamic functional connectivity and brain metastability during altered states of consciousness. Neuroimage 180 (Pt B), 383–395. doi:10.1016/j.neuroimage.2017.09.065.

. . . Chennu, S., Annen, J., Wannez, S., Thibaut, A., Chatelle, C., Cassol, H., Laureys, S., 2017. Brain networks predict metabolism, diagnosis and prognosis at the bedside in disorders of consciousness. Brain 140 (8), 2120–2132. doi:10.1093/brain/awx163.

. . . Chennu, S., Finoia, P., Kamau, E., Allanson, J., Williams, G.B., Monti, M.M., Bekinschtein, T.A., 2014. Spectral signatures of reorganised brain networks in disorders of consciousness. PLoS Comput. Biol. 10 (10), e1003887. doi:10.1371/journal.pcbi.1003887.

Ching, S., Cimenser, A., Purdon, P.L., Brown, E.N., Kopell, N.J., 2010. Thalamocortical model for a propofol-induced alpha-rhythm associated with loss of consciousness. Proc. Natl. Acad. Sci. U.S.A. 107 (52), 22665–22670. doi:10.1073/pnas.1017069108.

Colclough, G.L., Woolrich, M.W., Tewarie, P.K., Brookes, M.J., Quinn, A.J., Smith, S.M., 2016. How reliable are MEG resting-state connectivity metrics? Neuroimage 138, 284–293. doi:10.1016/j.neuroimage.2016.05.070.

. . . Duclos, C., Nadin, D., Mahdid, Y., Tarnal, V., Picton, P., Vanini, G., Blain-Moraes, S., 2021. Brain network motifs are markers of loss and recovery of consciousness. Sci. Rep. 11 (1), 3892. doi:10.1038/s41598-021-83482-9.

El-Baba, M., Lewis, D.J., Fang, Z., Owen, A.M., Fogel, S.M., Morton, J.B., 2019. Functional connectivity dynamics slow with descent from wakefulness to sleep. PLoS One 14 (12), e0224669. doi:10.1371/journal.pone.0224669.

Engel, A.K., Gerloff, C., Hilgetag, C.C., Nolte, G., 2013. Intrinsic coupling modes: multiscale interactions in ongoing brain activity. Neuron 80 (4), 867–886. doi:10.1016/j.neuron.2013.09.038.

Fedele, T., Blagovechtchenski, E., Nazarova, M., Iscan, Z., Moiseeva, V., Nikulin, V.V., 2016. Long-Range Temporal Correlations in the amplitude of alpha oscillations predict and reflect strength of intracortical facilitation: combined TMS and EEG study. Neuroscience 331, 109–119. doi:10.1016/j.neuroscience.2016.06.015.

. . . Finn, E.S., Shen, X., Scheinost, D., Rosenberg, M.D., Huang, J., Chun, M.M., Constable, R.T., 2015. Functional connectome fingerprinting: identifying individuals using patterns of brain connectivity. Nat. Neurosci. 18 (11), 1664–1671. doi:10.1038/nn.4135.

Gramfort, A., Papadopoulo, T., Olivi, E., Clerc, M., 2010. OpenMEEG: open-source software for quasistatic bioelectromagnetics. Biomed. Eng. Online 9, 45. doi:10.1186/1475-925x-9-45.

. . . Guggisberg, A.G., Rizk, S., Ptak, R., Di Pietro, M., Saj, A., Lazeyras, F., Pignat, J.M., 2015. Two intrinsic coupling types for resting-state integration in the human brain. Brain Topogr. 28 (2), 318–329. doi:10.1007/s10548-014-0394-2.

Helfrich, R.F., Knepper, H., Nolte, G., Sengelmann, M., Konig, P., Schneider, T.R., Engel, A.K., 2016. Spectral fingerprints of large-scale cortical dynamics during ambiguous motion perception. Hum. Brain Mapp. 37 (11), 4099–4111. doi:10.1002/hbm.23298.

. . . Imperatori, L.S., Betta, M., Cecchetti, L., Canales-Johnson, A., Ricciardi, E., Siclari, F., Bernardi, G., 2019. EEG functional connectivity metrics wPLI and wSMI account for distinct types of brain functional interactions. Sci. Rep. 9 (1), 8894. doi:10.1038/s41598-019-45289-7.

Imperatori, L.S., Cataldi, J., Betta, M., Ricciardi, E., Ince, R.A.A., Siclari, F., Bernardi, G, 2020. Cross-participant prediction of vigilance stages through the combined use of wPLI and wSMI EEG functional connectivity metrics. Sleep doi:10.1093/sleep/zsaa247.

Kim, H., Hudetz, A.G., Lee, J., Mashour, G.A., Lee, U., 2018. Estimating the integrated information measure phi from high-density electroencephalography during states of consciousness in humans. Front. Hum. Neurosci. 12, 42. doi:10.3389/fnhum.2018.00042.

. . . Kustermann, T., Ata Nguepnjo Nguissi, N., Pfeiffer, C., Haenggi, M., Kurmann, R., Zubler, F., De Lucia, M., 2020. Brain functional connectivity during the first day of coma reflects long-term outcome. Neuroimage Clin 27, 102295. doi:10.1016/j.nicl.2020.102295.

Kybic, J., Clerc, M., Abboud, T., Faugeras, O., Keriven, R., Papadopoulo, T., 2005. A common formalism for the integral formulations of the forward EEG problem. IEEE Trans. Med. Imaging 24 (1), 12–28. doi:10.1109/tmi.2004.837363.

Larremore, D.B., Shew, W.L., Restrepo, J.G., 2011. Predicting criticality and dynamic range in complex networks: effects of topology. Phys. Rev. Lett. 106 (5), 058101. doi:10.1103/PhysRevLett.106.058101.

. . . Lee, H., Golkowski, D., Jordan, D., Berger, S., Ilg, R., Lee, J., Lee, U., 2018. Relationship of critical dynamics, functional connectivity, and states of consciousness in large-scale human brain networks. Neuroimage 188, 228–238. doi:10.1016/j.neuroimage.2018.12.011.

Lee, H., Mashour, G.A., Noh, G.J., Kim, S., Lee, U., 2013a. Reconfiguration of network hub structure after propofol-induced unconsciousness. Anesthesiology 119 (6), 1347–1359. doi:10.1097/ALN.0b013e3182a8ec8c.

Lee, U., Ku, S., Noh, G., Baek, S., Choi, B., Mashour, G.A., 2013b. Disruption of frontal-parietal communication by ketamine, propofol, and sevoflurane. Anesthesiology 118 (6), 1264–1275. doi:10.1097/ALN.0b013e31829103f5.

Li, D., Vlisides, P.E., Kelz, M.B., Avidan, M.S., Mashour, G.A., 2019. Dynamic cortical connectivity during general anesthesia in healthy volunteers. Anesthesiology 130 (6), 870–884. doi:10.1097/aln.0000000000002656.

Linkenkaer-Hansen, K., Nikulin, V.V., Palva, J.M., Kaila, K., Ilmoniemi, R.J., 2004. Stimulus-induced change in long-range temporal correlations and scaling behavior of sensorimotor oscillations. Eur. J. Neurosci. 19 (1), 203–211. doi:10.1111/j.1460-9568.2004.03116.x.

Linkenkaer-Hansen, K., Monto, S., Rytsala, H., Suominen, K., Isometsa, E., Kahkonen, S., 2005. Breakdown of long-range temporal correlations in theta oscillations in patients with major depressive disorder. J. Neurosci. 25 (44), 10131–10137. doi:10.1523/jneurosci.3244-05.2005.

. .. Maier, K.L., McKinstry-Wu, A.R., Palanca, B.J.A., Tarnal, V., Blain-Moraes, S., Basner, M., Kelz, M.B., 2017. Protocol for the reconstructing consciousness and cognition (ReCCognition) study. Front. Hum. Neurosci. 11, 284. doi:10.3389/fnhum.2017.00284.

. . . Mikulan, E., Hesse, E., Sedeño, L., Bekinschtein, T., Sigman, M., García, M.D.C., Ibáñez, A., 2018. Intracranial high-γ connectivity distinguishes wakefulness from sleep. Neuroimage 169, 265–277. doi:10.1016/j.neuroimage.2017.12.015.

. . . Montez, T., Poil, S.S., Jones, B.F., Manshanden, I., Verbunt, J.P., van Dijk, B.W., Linkenkaer-Hansen, K., 2009. Altered temporal correlations in parietal alpha and prefrontal theta oscillations in early-stage Alzheimer disease. Proc. Natl. Acad. Sci. U.S.A. 106 (5), 1614–1619. doi:10.1073/pnas.0811699106.

Monto, S., Vanhatalo, S., Holmes, M.D., Palva, J.M., 2007. Epileptogenic neocortical networks are revealed by abnormal temporal dynamics in seizure-free subdural EEG. Cereb. Cortex 17 (6), 1386–1393. doi:10.1093/cercor/bhl049.

Mostame, P., Babajani-Feremi, A., Sadaghiani, S., 2019. Phase- and amplitude-coupling are two distinct but spatially associated modes of connectivity: an intracranial EEG study. Conference Program of 2019 Neuroscience Meeting Planner. Society for Neuroscience 2019.

. . . Mukamel, E.A., Pirondini, E., Babadi, B., Wong, K.F., Pierce, E.T., Harrell, P.G., Purdon, P.L., 2014. A transition in brain state during propofol-induced unconsciousness. J. Neurosci. 34 (3), 839–845. doi:10.1523/jneurosci.5813-12.2014.

. . . Nadin, D., Duclos, C., Mahdid, Y., Rokos, A., Badawy, M., Létourneau, J., Blain–Moraes, S., 2020. Brain Network Motif Topography May Predict Emergence from Disorders of consciousness: a Case Series Neurosci Conscious. *2020*(1), niaa017. doi:10.1093/nc/niaa017.

Nikulin, V.V., Brismar, T., 2004. Long-range temporal correlations in alpha and beta oscillations: effect of arousal level and test-retest reliability. Clin. Neurophysiol. 115 (8), 1896–1908. doi:10.1016/j.clinph.2004.03.019.

Nikulin, V.V., Brismar, T., 2005. Long-range temporal correlations in electroencephalographic oscillations: relation to topography, frequency band, age and gender. Neuroscience 130 (2), 549–558. doi:10.1016/j.neuroscience.2004.10.007.

. . . Purdon, P.L., Pierce, E.T., Mukamel, E.A., Prerau, M.J., Walsh, J.L., Wong, K.F., Brown, E.N., 2013. Electroencephalogram signatures of loss and recovery of consciousness from propofol. Proc. Natl. Acad. Sci. U.S.A. 110 (12). doi:10.1073/pnas.1221180110, E1142-1151..

. . . Ranft, A., Golkowski, D., Kiel, T., Riedl, V., Kohl, P., Rohrer, G., Ilg, R., 2016. Neural correlates of sevoflurane-induced unconsciousness identified by simultaneous functional magnetic resonance imaging and electroencephalography. Anesthesiology 125 (5), 861–872. doi:10.1097/aln.0000000000001322.

Sadaghiani, S., Wirsich, J., 2020. Intrinsic connectome organization across temporal scales: new insights from cross-modal approaches. Netw. Neurosci. 4 (1), 1–29. doi:10.1162/netn_a_00114.

Sanders, R.D., Tononi, G., Laureys, S., Sleigh, J.W., 2012. Unresponsiveness not equal unconsciousness. Anesthesiology 116 (4), 946–959. doi:10.1097/ALN.0b013e318249d0a7.

Shew, W.L., Plenz, D., 2013. The functional benefits of criticality in the cortex. Neuroscientist 19 (1), 88–100. doi:10.1177/1073858412445487.

Shew, W.L., Yang, H., Petermann, T., Roy, R., Plenz, D., 2009. Neuronal avalanches imply maximum dynamic range in cortical networks at criticality. J. Neurosci. 29 (49), 15595–15600. doi:10.1523/jneurosci.3864-09.2009.

Slezin, V.B., Korsakova, E.A., Dytjatkovsky, M.A., Schultz, E.A., Arystova, T.A., Sivola, J.R., 2007. Multifractal analysis as an aid in the diagnostics of mental disorders. Nord. J. Psychiatry 61 (5), 339–342. doi:10.1080/08039480701643175.

. . . Sripad, P., Rosenberg, J., Boers, F., Filss, C.P., Galldiks, N., Langen, K.J., Dammers, J., 2020. Effect of Zolpidem in the aftermath of traumatic brain injury: an MEG study. Case Rep. Neurol. Med. 2020, 8597062. doi:10.1155/2020/8597062.

Tadel, F., Baillet, S., Mosher, J.C., Pantazis, D., Leahy, R.M., 2011. Brainstorm: a user-friendly application for MEG/EEG analysis. Comput. Intell. Neurosci. 2011, 879716. doi:10.1155/2011/879716.

. . . Thiery, T., Lajnef, T., Combrisson, E., Dehgan, A., Rainville, P., Mashour, G.A., Jerbi, K., 2018. Long-range temporal correlations in the brain distinguish conscious wakefulness from induced unconsciousness. Neuroimage 179, 30–39. doi:10.1016/j.neuroimage.2018.05.06.

Vinck, M., Oostenveld, R., van Wingerden, M., Battaglia, F., Pennartz, C.M., 2011. An improved index of phase-synchronization for electrophysiological data in the presence of volume-conduction, noise and sample-size bias. Neuroimage 55 (4), 1548–1565. doi:10.1016/j.neuroimage.2011.01.055.

. . . Vlisides, P.E., Bel-Bahar, T., Lee, U., Li, D., Kim, H., Janke, E., Mashour, G.A., 2017. Neurophysiologic correlates of ketamine sedation and anesthesia: a high-density electroencephalography study in healthy volunteers. Anesthesiology 127 (1), 58–69. doi:10.1097/aln.0000000000001671.

Vlisides, P.E., Li, D., Zierau, M., Lapointe, A.P., Ip, K.I., McKinney, A.M., Mashour, G.A., 2019. Dynamic cortical connectivity during general anesthesia in surgical patients. Anesthesiology 130 (6), 885–897. doi:10.1097/aln.0000000000002677.

Zhang, Y., Wang, C., Wang, Y., Yan, F., Wang, Q., Huang, L., 2019. Investigating dynamic functional network patterns after propofol-induced loss of consciousness. Clin. Neurophysiol. 130 (3), 331–340. doi:10.1016/j.clinph.2018.11.028.